Graphical Abstract (for review)

Fault-slip data set

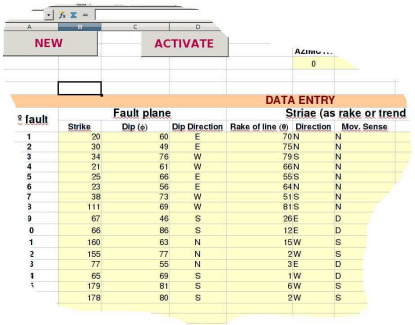

OpenOffice spreadsheet

y-R Diagram!!

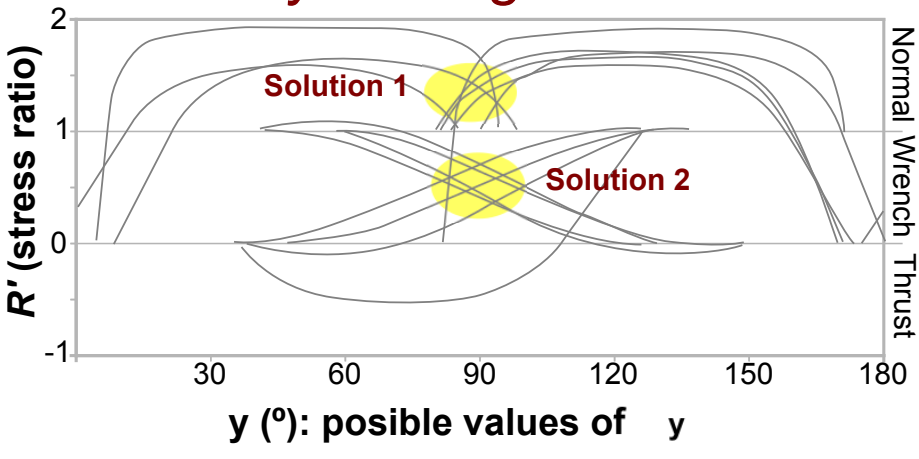

***Highlights (for review)**

Tool to calculate paleostress tensors from faults striations

A method to separate stresses from heterogeneous fault-slip data.

Graphic method which aids in recognizing different possible stress solutions.

The method allows to properly track the stress field analysis.

Title: *y*-g*R*aph: an OpenOffice application to reconstruct paleostress fields from striated faults

Authors:

Pablo Calvín[a,*], Pablo Santolaria[a], Pablo Tierz[a,b], Alicia Muñoz[a], Antonio Casas[a], Luis Arlegui[a], María A. Zapata[c].

a) Dpto. de Ciencias de la Tierra. Universidad de Zaragoza, C/ Pedro Cerbuna, 12, 50009 Zaragoza (Spain).

b) Istituto Nazionale di Geofisica e Vulcanologia, INGV, Sezione di Bologna, Via Donato Creti, 12, 40128 Bologna (Italy)

c) Dpto. Informática e Ingeniería de Sistemas. Universidad de Zaragoza, C/ Pedro Cerbuna, 12, 50009 Zaragoza (Spain).

*Corresponding author: Departamento de Ciencias de la Tierra. Universidad de Zaragoza, C/ Pedro Cerbuna 12, 50009 Zaragoza, Spain. Tel: 34-690789887, Fax: 34-976761106, E-mail: calvinballester@gmail.com

Abstract: *y*-g*R*aph, a user-friendly spreadsheet for reconstructing paleostress fields by means of the *y*-*R* diagram is presented. The *y*-*R* diagram is based on Bott´s equation and translates the parameters of the stress ellipsoid to a XY plot representing the maximum horizontal stress orientation (σ_y) and the stress ratio (*R*), compatible with a given set of striated faults. In cases where several stress tensors fit the dataset, *y*-*R* diagram aids in visualizing unrealistic solutions or changes in the stress field with time. Furthermore, the spreadsheet allows to rotate planes and lines, thus simplifying the work with tilted fault populations. Histograms and rose diagrams showing the strike of faults and

the trend of striae complement the *y*-g*R*aph main output. The application was built using Apache OpenOffice software and supports a variety of input data formats: (i) strike, dip and dip direction (SDD), (ii) azimuth and dip (AD) according to the "Right-hand rule", and (iii) dip and dip direction (DD).

Keywords: striae, fault analysis, stress tensors, brittle deformation, paleostress analysis.

1. Introduction

Stress analysis methods based on brittle structures started to develop in the late sixties and early seventies with the works presented by Arthaud (1969), Arthaud and Choukroune (1972) and Mattauer (1973). During the following decades, additional techniques were developed (Angelier, 1984, 1994; Fry, 1992; Ramsay and Lisle, 2000; Yamaji, 2000; Célérier and Séranne, 2001; Yamaji et al., 2006; Zalohar and Vrabec, 2007; Célérier et al., 2012) and some of them were based on Bott's (1959) equation. This equation relates the shear stress component on the fault plane (striation) to the reduced stress tensor (expressed by the orientation of the three principal axes $\sigma_1>\sigma_2>\sigma_3$, and the ratio between these axes, which defines the stress regime, Angelier, 1994). Casas-Sainz et al. (1990) reviewed some of the different methods in the literature and concluded that one of the most reliable procedure to calculate paleostress axes from faults with striae is the synergic use of (i) a kinematical approach (e.g.Right Dihedra; Angelier and Mechler, 1977) as a first approximation to the solution, (ii) a Bott´s based graphical approach (e.g.*y*-*R* diagram; Simón-Gómez, 1986; FSA; Célérier, 1998) in order to graphically establish a more accurate estimation as well as to display the spectrum of reduced stress tensors compatible with the fault population and (iii) an iterative numerical approach based on Bott's equation (e.g. Etchecopar´s method, Etchecopar et al., 1981, FSA; Célérier, 1998) to

explore the results suggested by the previous methods and to obtain more precisely defined tensors. This procedure has been used by many authors (e.g., Casas-Sainz and Simón-Gómez, 1992; Casas-Sainz and Maestro-González, 1996; Arlegui-Crespo and Simón-Gómez, 1998; Liesa and Simón, 2009, among others). However, the lack of a user-friendly software to perform the *y*-*R* diagram hindered its widespread use within the scientific community.

The *y*-*R* diagram is a particularly useful tool when a variety of stress fields are recorded within a region: this method displays the spectrum of possible solutions and thereby allows the identification of those faults related to different stress fields. In addition, it serves to properly track the intermediate stages of the paleostress analysis. In this paper, a user-friendly application (*y*-g*R*aph) that displays the *y*-*R* diagram associated to a given population of striated faults is presented.

2. Theoretical background

Under a specific stress regime, reactivation of pre-existing fault planes is frequently favoured compared to new-formed fault planes. This is especially observed in complex outcrops where the measured sets of faults may not be consistent with Anderson's theory of faulting. That fact can hinder the interpretation of the stress regime under which the faults were formed. However, by gathering measurements from a population of these reactivated planes/discontinuities (fault plane strike and striae with sense of movement), the orientation of the maximum shear stress acting on a plane can be mathematically inferred from Bott´s equation (1) (Bott, 1959; Célérier at al., 2012):

$$\tan\theta = [n / (lm)]\,[m^2 - (1 - n^2)\,R] \qquad (1)$$

where the stress ratio is $R = (\sigma_z - \sigma_x) / (\sigma_y - \sigma_x)$;

l, *m*, *n* are the direction cosines of the plane referred to the stress axes (σ_x, σ_y, σ_z) system and θ is the striation (resolved shear stress) rake on the fault plane. σ_z , σ_y and σ_x are the principal stress axes (eigenvectors of the stress matrix, (2)) in the xyz coordinate system, whose base vectors can be normalized (values between 0 and 1) according to the deviatoric stress tensor.

Based on a modified version of Bott´s equation (2) and considering that one of the main stress axes is vertical (σ_z), Simón-Gómez (1986) proposed the *y*-*R* diagram as a method to show the relation between two parameters: (i) *y*, the possible azimuth of $\sigma_y$and (ii) *R*, the stress ratio of the deviatoric stress tensor.

$$R = \sin^2\lambda - [(\tan\theta \sin 2\lambda) / 2\cos\phi] \qquad (2)$$

where λ is the angle between *y* and the azimuth (α) of the fault, therefore $\lambda = \alpha \pm y$ (it is added or subtracted according to the sense of movement: dextral or sinistral, respectively), ϕ is the fault dip and θ is the striation rake on the fault (Fig. 1). For each fault, there is a 90º range (from azimuth) which σ_y is compatible with the measured movement of the fault (rake and sense of movement) and therefore there are values of *y*-*R* (equal values of *R* correspond to y + 180)Those values, once plotted in the *y*-*R* diagram, draw a curve per each fault measured in the set.

The *y*-*R* method assumes that one of the principal axes is vertical, which is, under brittle conditions, a common tendency in nature (Lisle et al., 2006; Liesa and Simón, 2009); this simplification is the basis of the method since it allows stress states to be represented by the *y*-*R* values compatible with each fault, defining a curve on a 2D diagram. The “knots” where the curves intersect show a preliminary range of possible solutions for the azimuth of σ_y (*y*) and *R* under which the faults could have moved. However, due to this simplification (one of the stress axes is vertical), it is essential to couple *y*-*R* diagram to other 3D methods since, even though it is expected that one of the stress axes

was vertical during the slipping time, faults may have been tilted after their formation. A complementary method to deal with tilted fault systems is also included in *y*-g*R*aph.

3. Spreadsheet description

y-g*R*aph is written as a spreadsheet template using the free software suite Apache OpenOffice. This spreadsheet consists of nine worksheets (Fig. 2):

- **Instructions** worksheet.

- The **Input data** block is divided into three different worksheets (SDD, AD and DD). Their differences only involve data input format according to the user's preferences.

- In the "**Graph"** worksheet the *y*-*R* diagram corresponding to the fault population is generated.

- "**Extras"** worksheet contains graphics (rose diagram and histogram) representing the strike of faults and trend of striae in order to assist in the interpretation.

- "***y*-*R* calculation"** worksheet includes the automatic calculations which generate the *y*-*R* diagram.

- "**Fault rotation"** worksheet performs automatic computations to define the coordinates of fault vectors in a rotated reference system (i.e., faults are rotated according to its bedding orientation).

3.1 Data input

Three formats of fault data entry can be used (strike, dip and dip direction; azimuth and dip; dip and dip direction). Each one can be found in a different worksheet labelled as "SDD", "AD" and "DD", respectively. Striae data may be introduced as the rake of the line on the measured plane or as trend and plunge. More precise specifications about data entry format are available in the Introduction

worksheet and in the User´s guide.

Data entry section (A to J columns in SDD, A to I AD and DD worksheets) receives the raw data from the user. The "NEW" button in the "Input data" worksheets must be used if the user wants to clean the input cells. This button has an associated macro that deletes all the values in the data entry section, restoring the section to default.

"Data revision" section is available in all the "Input data" worksheets (L to S columns in "SDD", K to Q in "AD" and "DD" worksheets). In this section, an "IF" function evaluates the consistency of the data, eventually displaying a "review" label if data incompatibility is found.

The single goal of the "Automatic Computation" section (AE to AS columns in "SDD", AB to AP in "AD", AC to AQ in "DD" worksheets) is to standardize the introduced data. The standard data format is established as azimuth (0 to 2π radians) and dip (0 to $\pi/2$ radians) for fault planes and rake (0 to π radians measured from the azimuth on the fault plane) and movement sense (in horizontal component D or S) for striae (rakes of 90º are considered by the application as 89.9999). If the striae orientations have a trend/plunge format, this section converts these data, by vector calculation (3), to standard rake format (AE to AJ columns in "ADD" worksheet.)

$$\cos\theta = (a_1 * b_1 + a_2 * b_2 + a_3 * b_3) / [\sqrt{(a_1^2 + a_2^2 + a_3^2)} * \sqrt{(b_1^2 + b_2^2 + b_3^2)}] \qquad (3)$$

where a_1, a_2, a_3 are the vector components of the azimuth in the Cartesian reference system (x, y, z in North, East and vertical directions, respectively; a_3 is always 0) and b_1, b_2, b_3 are the vector components of the striae.

In any case, the rake is modified to the standard format (rake measured from the azimuth) by means of an "IF" function which compares the azimuth, the direction from where the striae have been measured and the original rake ("Rake [from α]"). When rake equals 0º or 180º, a value of 10^{-6}

degrees is added or subtracted, respectively, in order to prevent divisions by zero (”Rake [without 0 and 180]” row). “Azimuth (α)” column compares the strike and dip sense to calculated azimuth. The “movement sense (D or S)” column compares the rake of the striation and the original sense of movement in order to assign one of two single components (dextral and sinistral; 90º values of rake should be avoided). Degrees are converted to radians (“Conversion to radians” columns) which is the angle format that OpenOffice functions take as input argument.

Furthermore, three parameters to rotate the data should be entered in this worksheet (F1:M3): azimuth of the rotation axis, magnitude of rotation and sense of rotation (clockwise or counter-clockwise) according to the introduced azimuth.

The analysed data should be available for all the following calculations. For that reason, the “Activate” button writes the active worksheet name (SDD, AD or DD) in ‘Fault Rotation’ G3 cell. This cell acts as a marker for the incoming data in the Fault rotation and Graph worksheets.

3.2 Fault rotation

y-g*R*aph allows the faults and striae to be tilted according to a specified rotation axis. Calculations are carried out in “Fault rotation” worksheet: “Original data” section takes the data from the activated “Input data” worksheet where the user has already introduced the parameters of the rotation axis. The “Fault rotation” worksheet picks up the standard data placed at the automatic computation section (see above) in the activated “Input data” worksheet.

The routine to rotate the data is based upon vector analysis (Spiegel, 1998; Casas-Sainz et al., 2005). Each fault is represented by the unit director vector of the fault plane (always pointing downwards) and the unit vector for the striation. Rotation is accomplished according to coordinate transformation from the initial reference system (x, y, z in North, East and vertical directions, respectively) to a new reference system (defined by (i) the rotation direction, (ii) the perpendicular

to the correction plane defined by the amount of rotation and (iii) a third vector corresponding to the dip direction of the correction plane). Just to simplify calculations, two vertical axes rotations are performed before and after the change of reference system. In the first one, the x axis of the new reference system is set to a North position as the whole dataset is rotated consequently. In the second, x axis is returned to its starting position through vertical axis rotation (after tilting of the dataset). Details of the equations that are deduced from the transformation matrix product can be obtained in Casas-Sainz et al. (2005).

In "Fault rotation" worksheet all the calculations that are needed to rotate the faults are organized in three different modules. In the first module (H7:AB108), unit director vectors of both the fault and the striae are calculated (V7:X108 and Z7:AB108, respectively). In the second module (AC7:BR108), the unit director vector of the rotation axis is calculated. In the third module (BS7:DV108), once the orientations of vectors in the rotated reference system are calculated, IF routines allow to translate Cartesian to geological coordinates (Fisher et al., 1987) as well as assign the sense of dip, rake and sense of movement to each fault. Data from rotated faults (DY to EK columns) will be used in the subsequent calculation processes. These data are also displayed in the "Input data" worksheets ("Rotated faults" columns in the corresponding "Input data" worksheet).

3.3. Calculation of *y*-*R* pairs of values

y-*R* calculations worksheet is the main body of the application. *y* and *R* values are calculated here. To solve Bott's modified equation (2) several steps are considered:

i) The rotated faults obtained in the previous process are imported to the "Rotated fault data" section (A to H columns) and degrees are converted to radians.

ii) λ values ($0 \leq y \leq 360$; cells K5:NH107) are calculated for every *y* compatible value in one degree intervals.

$\lambda = \alpha + y$ (if the horizontal component of the fault is dextral) (4)

$\lambda = \alpha - y$ (if the horizontal component of the fault is sinistral) (5)

An "IF" function checks the movement sense (D or S) and the relation between y and the azimuth α to calculate λ values by means of equations (4) or (5).

iii) R value ($0 \leq y \leq 360$; $-\infty < R < \infty$; cells NK5:ABH107). Another "IF" function recognizes the interval of y values for which λ has been calculated. Inside this valid interval, R values are calculated through (2).

iv) Duplicated R values ($0 \leq y \leq 360$; $-\infty < R < \infty$; cells K110:NH212). As we are dealing with axes, duplicated R values are calculated for the opposite quadrant (y + 180º). An "IF" function allows to obtain the duplicated R values.

v) Duplicated R' values ($0 \leq y \leq 3$ 60; $-1 \leq R \leq 2$; cells NK110:ABH212): In order to use a bounded graphic interval, the ordinate axis, R, with support in$(-\infty, +\infty)$, is modified by R', with support in [-1, 2] as follows (6):

if $R < 0$; $R' = -R / (R - 1)$

if $0 \leq R \leq 1$; $R' = R$

if $R > 1$; $R' = 1 + [(R - 1) / R]$ (6)

Doing so, the y-R diagram is compartmented to three equally sized intervals along the ordinate axis, limited by fixed R' values which correspond to the main stress regimes: thrust regime from -1 to 0,

wrench regime from 0 to 1 and normal regime from 1 to 2.

3.4 Graph

The main goal of *y*-g*R*aph application is to represent the *y*-*R* diagram in the "Graph" worksheet. To do so, the data coming from the "*y*-*R* calculations" is imported here (AH:OE columns). The *y*-*R* diagram is a XY chart where faults are represented as curves in the 1º-180º domain (users may edit this domain within others intervals). Every fault can be displayed or hidden by clicking its corresponding checkbox (which is linked to an OF column, generating a marker for each fault) beside the graph. These markers are used by *R'* cells (AI4:OF103) to display or hide the values. To facilitate the interpretation of the diagram, "Observations" (Q column), "Rotated faults" (R:Y columns) and "Original faults" (AA:AF columns) are also shown here. Note that 'Fault Rotation' G3-marker points out the data format to be imported into "Graph" worksheet. Rotation parameters and input data format are also shown (D36:I38 and K37:M38 cells respectively).

3.5 Extras

The "Extras" worksheet includes several graphs which may help in the interpretation of the *y*-*R* diagram. Two paired histogram-Rose diagrams showing the strike of the faults and the trend of the striae are displayed. A double smoothing procedure is performed to enhance the signal-to-noise ratio (Wise and McCrory, 1982). From columns N to R; the frequency of the strike of the faults is calculated and then the double smoothing is applied. Finally, frequency is expressed as a percentage normalized by the number of faults. The strike is also displayed in a symmetric rose diagram (with a range from 0 to 360º), using data from T to X columns. Finally, in columns Y to AF, the orientations of the striae are smoothed in the same way as the strike (but considering 360º).

4. Practical example and secondary applications

After measuring and introducing the data, *y*-g*R*aph application plots a diagram where each fault is represented by one curve (Fig. 3). The results obtained can be ascribed to one of three typical cases: (i) most of the curves intersect at a knot, indicating an optimal solution for a majority of the faults (Fig. 3a); (ii) two or more sets of faults intersect at different knots (note that a particular curve (fault) cannot belong to two different knots, i.e., it could not move, simultaneously, under two different stress fields; Fig. 3b), which are indicative of different stress states recorded in the outcrop (Liesa and Simón, 2009), and (iii) there is no defined knot, and the intersections between curves are distributed in an elongated area (Fig. 3c), defining a continuous temporal evolution of the stress field (Simón-Gómez, 1986).

Casas-Sainz and Simón-Gómez (1992) proposed another use of the *y*-*R* diagram based on the relationship between small-scale faults and major geological structures through the pattern of stress axes distribution in map view. This method can be applied to both compressional (Casas et al., 1992; Casas-Sainz and Simón-Gómez, 1992; Martínez-Peña et al., 1995; Casas-Sainz and Maestro-González, 1996) and extensional (Mattei et al., 1997; Cifelli et al., 2007) tectonic settings. Firstly, the regional orientations of the paleostress axes and the stress ratio (*R*) are estimated using the diagram with data collected from many outcrops. Secondly, the strike and dip of the main faults contemporary to the minor structures are utilized to infer the rake (which indicates the kinematics of the fault) of the theoretical striation on this major fault, and that can be used to calculate the stress field under which it should have moved. Eventually, it is possible to predict the orientation of the expected striations and find out the kinematics of the main fault, which can be compared to field indicators (cleavage or striations on the main fault surface). In a similar way, Lafuente-Tomás (2011) analysed the possible pattern of displacement on a large normal fault with changes in strike and dip.

The *y*-*R* diagram also provides an interesting way of displaying the set of solutions of paleostress tensors obtained in regional studies (Casas-Sainz and Maestro-González, 1996; Fig. 3d). Finally, if the evolution of the stress states in the region is know, it is possible to assign a given group of brittle structures to a specific stress field, or the *y*-*R* diagram can aid in visualizing the temporal changes in the stress field (Simón-Gómez, 1986; Fig. 3d).

Fig. 4 shows a comparison between different paleostress methods: Right Dihedra (Angelier and Mechler, 1977); Etchecopar´s method (Etchecopar et al., 1981) FSA (Célérier, 1998), Gauss method (Zalohar and Vrabec, 2007) and *y*-g*Raph* diagram. The Right Dihedra method gives a first approximation to the stress axes directions while the other methods offer more detailed information: e.g., two sets of faults related to two different stress solutions. The *y*-g*R*raph diagram allows to analyse graphically the compatibility between different fault sets.

5. Conclusions

An application (*y*-*gRaph*) to reconstruct paleostress fields from faults striations by means of the *y*-*R* diagram method is here presented. Based on modified Bott´s equation, the diagram relates *y* (azimuth of the maximum horizontal stress axis) and *R* (stress ratio) to a measured population of striated faults. Beyond the usual paleostress determination, this method is very useful when a variety of stress tensors is recorded within a fault population or to summarize the distribution and evolution of stress fields in a regional survey.

y-g*R*aph can be freely downloaded from here.

Appendix

Nº fault	Fault plane			Striae (as rake or trend and plunge)		
	Strike	Dip (ϕ)	Dip Direction	Rake of line (θ)	Direction	Mov. Sense
1	40	63	W	13	N	S
2	163	86	W	3	S	D
3	37	84	W	14	N	S
4	25	83	E	11	N	S
5	38	85	E	7	N	S
6	148	72	W	16	S	D
7	176	81	W	3	S	D
8	31	86	W	4	N	S
9	35	86	E	17	N	S
10	31	85	W	7	N	S
11	34	88	W	6	N	S
12	31	84	E	12	N	S
13	157	75	W	1	N	D
14	21	86	W	6	N	S
15	170	86	W	2	S	D
16	177	71	W	10	S	D
17	30	73	W	22	N	S
18	173	87	W	4	S	D
19	157	84	W	13	S	D
20	158	75	W	10	N	D
21	162	87	E	4	N	D
22	36	87	W	7	S	S
23	174	79	W	22	S	D
24	97	80	S	87	E	N
25	178	79	E	9	N	D
26	10	54	W	76	S	N
27	146	72	W	6	N	¿?
28	11	82	E	80	N	N
29	167	75	W	3	N	D

30	161	82	E	8 S	D
31	144	83	W	2 N	D
32	47	88	E	22 N	S
33	172	88	W	4 N	D
34	168	75	W	2 N	D
35	159	83	W	2 S	D
36	39	80	W	6 N	S
37	152	86	W	27 N	D
38	13	82	E	87 S	N
39	176	82	W	7 S	D
40	160	71	W	3 S	D
41	26	67	W	4 N	S
42	30	42	W	77 S	N
43	24	77	W	4 S	¿?
44	25	90	E	11 N	S
45	28	86	W	10 N	S
46	31	81	W	4 S	D
47	158	86	W	4 S	D
48	145	87	E	3 S	D
49	157	77	W	5 N	D
50	161	86	W	18 S	D
51	162	75	W	10 S	D
52	172	86	W	13 S	D
53	162	82	E	3 S	D
54	155	81	W	4 S	D
55	42	85	W	18 N	S
56	45	86	W	3 S	S
57	18	89	E	13 N	S
58	40	75	W	5 S	S
59	12	68	E	78 N	N
60	169	81	E	32 S	D
61	164	81	W	9 S	D
62	177	84	W	1 S	D
63	170	82	W	15 S	D
64	42	78	W	5 S	D

65	167	84 W	1 S	D
66	177	89 W	25 N	D
67	158	89 W	11 N	D
68	51	84 W	11 S	S
69	48	79 W	3 S	S
70	170	85 W	24 N	D
71	34	78 E	14 S	S
72	8	71 W	58 N	N
73	176	78 E	32 N	D
74	22	79 E	4 S	D
75	44	85 E	8 N	S
76	36	81 W	12 N	S
77	35	88 E	6 N	S
78	8	83 E	10 N	D
79	35	75 E	6 N	¿?
80	176	77 E	35 S	D

References

Angelier, J., 1984. Tectonic analysis of fault slip data sets, Journal of Geophysical Research, 89(B7), 5835–5848.doi: 10.1029/JB089iB07p05835.

Angelier, J., 1994. Fault slip analysis and palaeostress reconstruction. In Continental deformation (Ed. Handcock), Pergamon Press, Oxford, pp. 53–100.

Angelier, J., Mechler, P. (1977), Sur une méthode graphique de recherche des contraintes principales également utilisable en tectonique et en séismologie: le méthode des diedres droits. Bulletin de la Societé Géologique de France 19, 1309-1328 [in French].

Arlegui-Crespo, L.E., Simón-Gómez, J.L., 1998. Reliability of paleostress analysis from faults striations in near multidirectional extension stress fields. Example from the Ebro Basin, Spain. Journal of Structural Geology 20, 827-840. doi: 10.1016/S0191-8141(98)00012-1.

Arthaud, F. (1969). Méthode de détermination graphique des directions de raccourcissement, d'allongement et intermédiaire d'une population de failles. Bulletin de la Societé Géologique de France, 7 (11), 729-737 [in French].

Arthaud, F., Choukroune, P. (1972). Méthode d'analyse de la tectonique cassante a I'aide des microstructures dans les zones peu deformées. Example de la plateforme Nord-Aquitaine. Revue de l'Institut Francais du Pétrole., 27 (5), 715-732 [in French].

Bott, M.H.P., 1959. The mechanics of oblique slip faulting. Geological Magazine 96, 109-117. doi: 10.1017/S0016756800059987.

Casas-Sainz, A.M., Gil-Peña, I., Simón-Gómez, J.L., 1990. Los métodos de análisis de paleoesfuerzos a partir de poblaciones de fallas: sistemática y técnicas de aplicación. Estudios

geológicos 46, 385-398 [in Spanish].

Casas, A.M., Simón, J.L., Serón, F.J., 1992. Stress deflection in a tectonic compressional field: a model for the Northwestern Iberian Chain, Spain. Journal of Geophysical Research 97 (B5), 7183-7192. doi: 10.1016/0191-8141(92)90154-O.

Casas-Sainz, A.M., Simón-Gómez, J.L., 1992. Stress field and thrust kinematics: a model for the tectonic inversion of the Cameros Massif (Spain). Journal of Structural Geology 14, 521-530. doi: 10.1016/0191-8141(92)90154-O.

Casas-Sainz, A.M., Maestro-González, A., 1996. Deflection of a compressional stress field by large-scale basement faults. A case study from the Tertiary Almazán basin (Spain). Tectonophysics 255, 135-156. doi: 10.1016/0040-1951(95)00111-5.

Casas-Sainz. A.M., Soto-Marín, R., Gonzalez, A., Villalaín., J.J., 2005. Folded onlap geometries: implications for recognition of synsedimentary folds. Journal of Structural Geology, 27, 1644-1657. doi: 10,1016/j.jsg.2005.05.005.

Célérier, B., 1998. FSA: Fault & Stress Analysis software, version 19.0, http://www.pages-perso-bernard-celerier.univ-montp2.fr/software/dcmt/fsa/fsa.html.

Célérier, B., M. Séranne, 2001. Breddin's graph for tectonic regimes. Journal of Structural Geology, 23, 789–801, doi: 10.1016/S0191-8141(00)00140-1 & doi: 10.1016/S0191-8141(01)00058-X.

Célérier,B., Etchecopar, A., Bergerat, F., Vergely, P., Arthaud, F., Laurent, P., 2012. Inferring stress from faulting: From early concepts to inverse methods, Tectonophysics, 581, 206–219, doi: 10.1016/j.tecto.2012.02.009

Cifelli, F., Rosseti, F., Mattei, M., 2007. The architecture of brittle postorogenic extension: Results from an integrated structural and paleomagnetic study in north Calabria (southern Italy). Geological Society of American Bulletin 119, 221-239. doi:10.1130/B25900.1.

Etchecopar, A., Vasseur, G., Daignières, M., 1981. An inverse problem in microtectonics for the determination of stress tensors from fault striation analysis. Journal of Structural Geology 3, 51-65. doi: 10.1016/0191-8141(81)90056-0.

Lafuente-Tomás, P., 2011. Tectónica activa y paleosismicidad de la falla de Concud (Cordillera Ibérica central). PhD Thesis, Univ. Zaragoza, Spain, [in Spanish] 272pp.

Liesa, C.L., Simón, J.L., 2009. Evolution of intraplate stress fields under multiple remote compressions: .The case of the Iberian Chain (NE Spain). Tectonophysics 474, 144-159. doi: 10.1016/j.tecto.2009.02.002.

Lisle, R.J., Orife, T.O., Arlegui, L., Liesa, C., Srivastava, D.C., 2006. Favoured states of palaeostress in the Earth's crust: evidence from fault-slip data. Journal of Structural Geology 28, 1051-1066. doi: 10.1016/j.jsg.2006.03.012.

Martínez-Peña, M.B., Casas-Sainz, A.M., Millán-Garrido, H., 1995. Reply-Palaeostress associated with thrust sheet emplacemente and related folding in the southern central Pyrenees, Huesca, Spain. Journal of the Geological Society 152, 1053-1054. doi: 10.1144/GSL.JGS.1995.152.01.28

Mattauer, M., 1973. Les déformations des matériaux de l'ecorce terrestre, Hermann. Paris, [in French] 493 pp.

Mattei, M., Sagnotti, L., Faccenna, C., Funiciello, R., 1997. Magnetic fabric of weakly deformed clayey sediments in the Italian peninsula: relationships with compressional and extensional tectonics. Tectonophysics 271, 107–122. doi: 10.1016/S0040-1951(96)00244-2.

Ramsay, J.G., R. Lisle, R. 2000. The techniques of modern structural geology; Volume 3: Applications of Continuum Mechanics in Structural Geology, Academic Press, London. pp. 701-1061.

Simón-Gómez, J.L., 1986. Analysis of a gradual change in stress regime (example from the Eastern

Iberian Chain, Spain). Tectonophysics 124, 37-53. doi: 10.1016/0040-1951(86)90136-8.

Spiegel, M.R., 1998. Schaum's Mathematical Handbook of Formulas and Tables, McGraw-Hill, New York, 278pp.

Yamaji, A., 2000. The multiple inverse method: a new technique to separate stresses from heterogeneous fault-slip data, Journal of Structural Geology, 22, 441-452. doi: 10.1016/S0191-8141(99)00163-7.

Yamaji, A., Otsubo, M., Sato, K., 2006. Paleostress analysis using the Hough transform for separating stresses from heterogeneous fault-slip data, Journal of Structural Geology, 28, 980–990. doi: 10.1016/j.jsg.2006.03.016.

Wise, D., McCrory, T.A., 1982. A new method of fracture analysis: Azimuth versus traverse distance plots. Geological Society of America Bulletin, 9, 889-897. doi: 10.1130/0016-7606(1982)93.

Zalohar, J., Vrabec, M., 2007. Paleostress analysis of heterogeneous fault-slip data: The Gauss method, Journal of Structural Geology, 29, 1798–1810. doi: 10.1016/j.jsg.2007.06.009.

Figure Captions:

Fig. 1. Defining parameters of the converted Bott's equation. σ_z: vertical principal stress direction; σ_y: maximum horizontal principal stress direction; λ: angle between azimuth and σ_y; θ: rake; Φ: plunge. The possible range of directions of the maximum horizontal stress axis σ_y (90° from the azimuth of the fault counted clockwise or counter-clockwise depending on whether the fault is dextral or sinistral respectively) is represented by the dashed line included in the horizontal plane (note that the depicted fault is sinistral).

Fig. 2. Flow diagram showing the sequence of operations performed by the application. Circles indicate input data sections, squares indicate automated calculations performed by the application and diamonds indicate output data or diagrams.

Fig. 3. Example of *y*-*R* diagrams in paleostress analysis. (a) Single solution. (b) Two solutions for two different sets of faults. (c) Complex solution: the knots show an elongated and continuous sector than can be interpreted as a continuous temporal evolution of stress states; indicators such as the presence of more than one set of striations in the same fault planes or others can be very useful to corroborate this interpretation. (d) *y*-*R* diagram showing the different solutions obtained in the subsites of a region, and temporal evolution of the stress field.

Fig. 4. Example of paleostress analysis from fault slip data using and comparing different methods over the *y*-*R* diagram. Data from 81 real faults used for it are included in the Appendix. Star: Etchecopar's method; square: FSA method; diamond: Gauss method.

Figure(s)

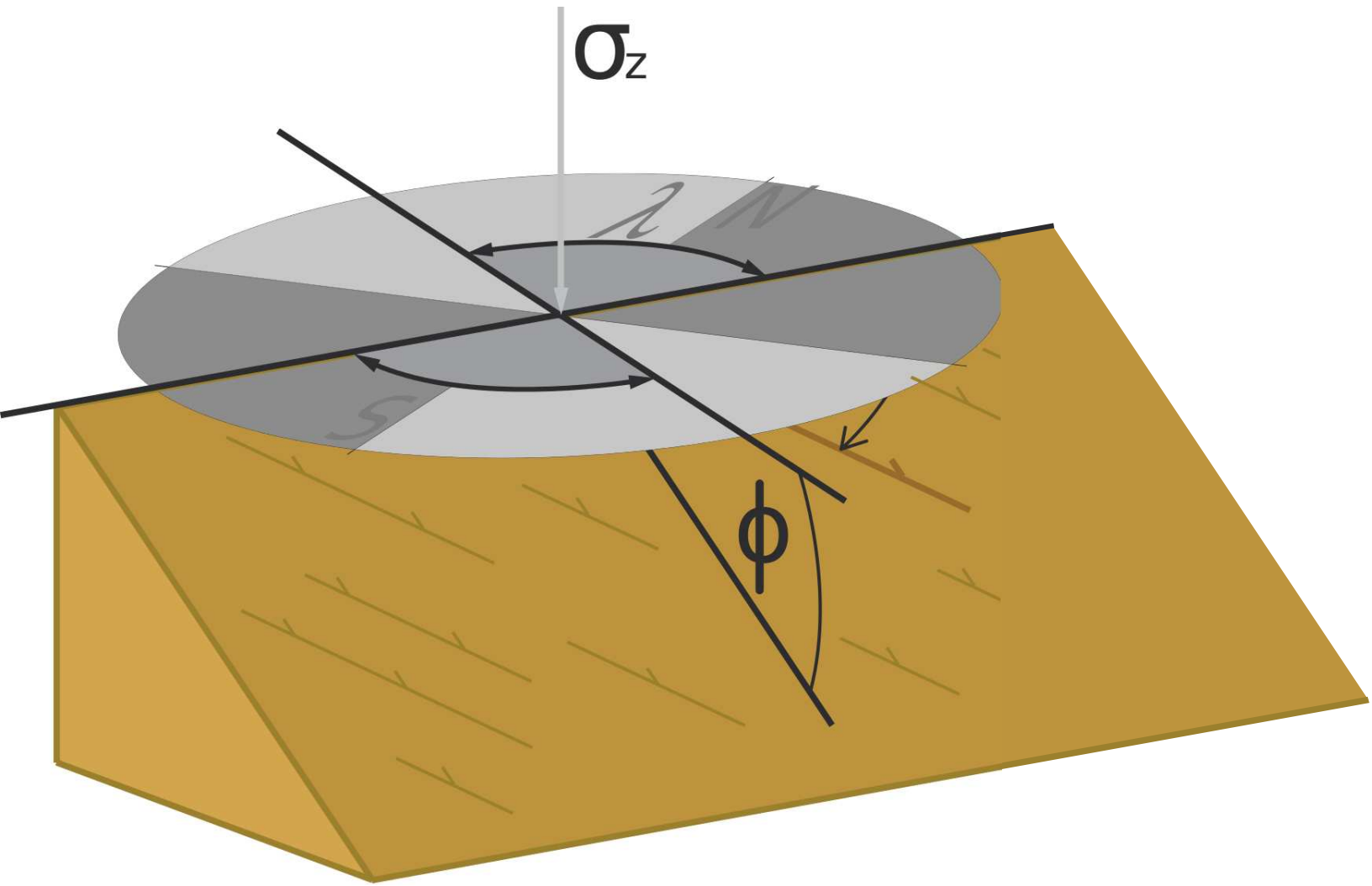

Figure(s)

Click here to download high resolution image

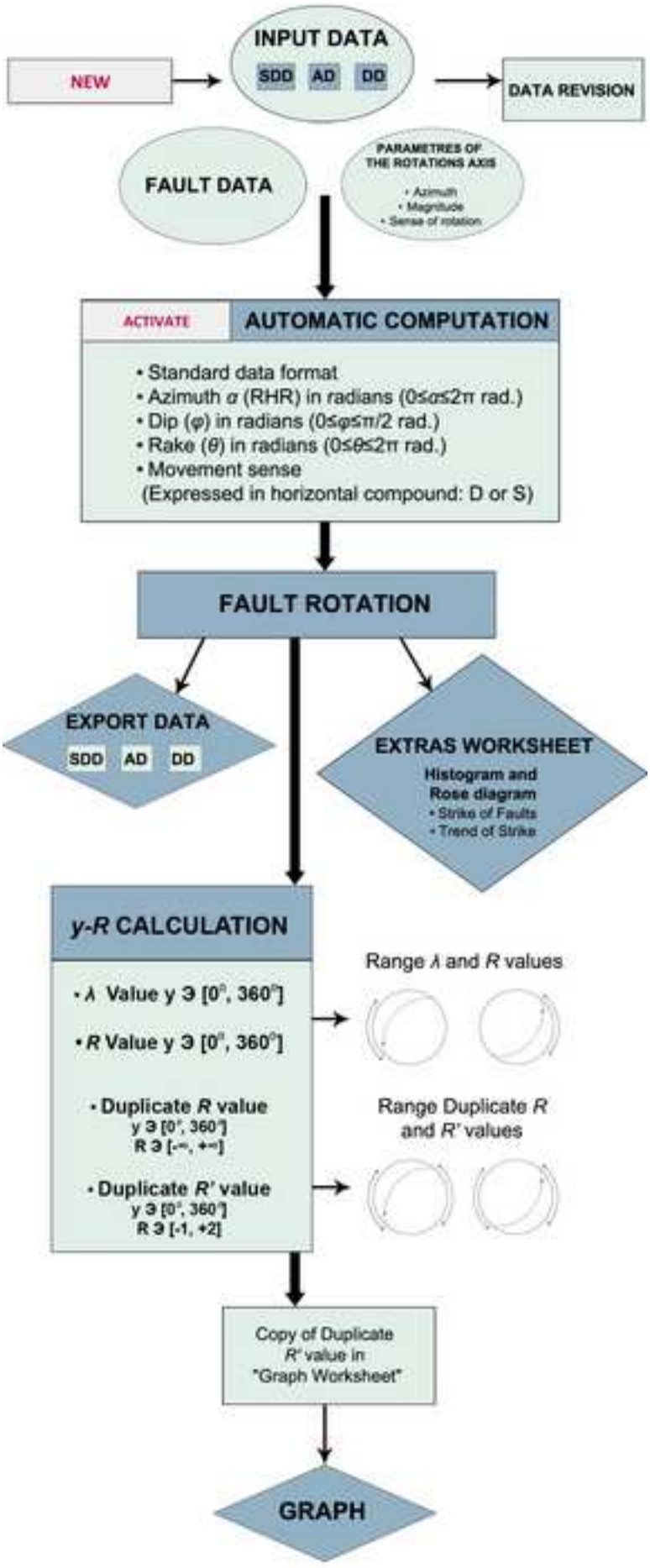

Figure3

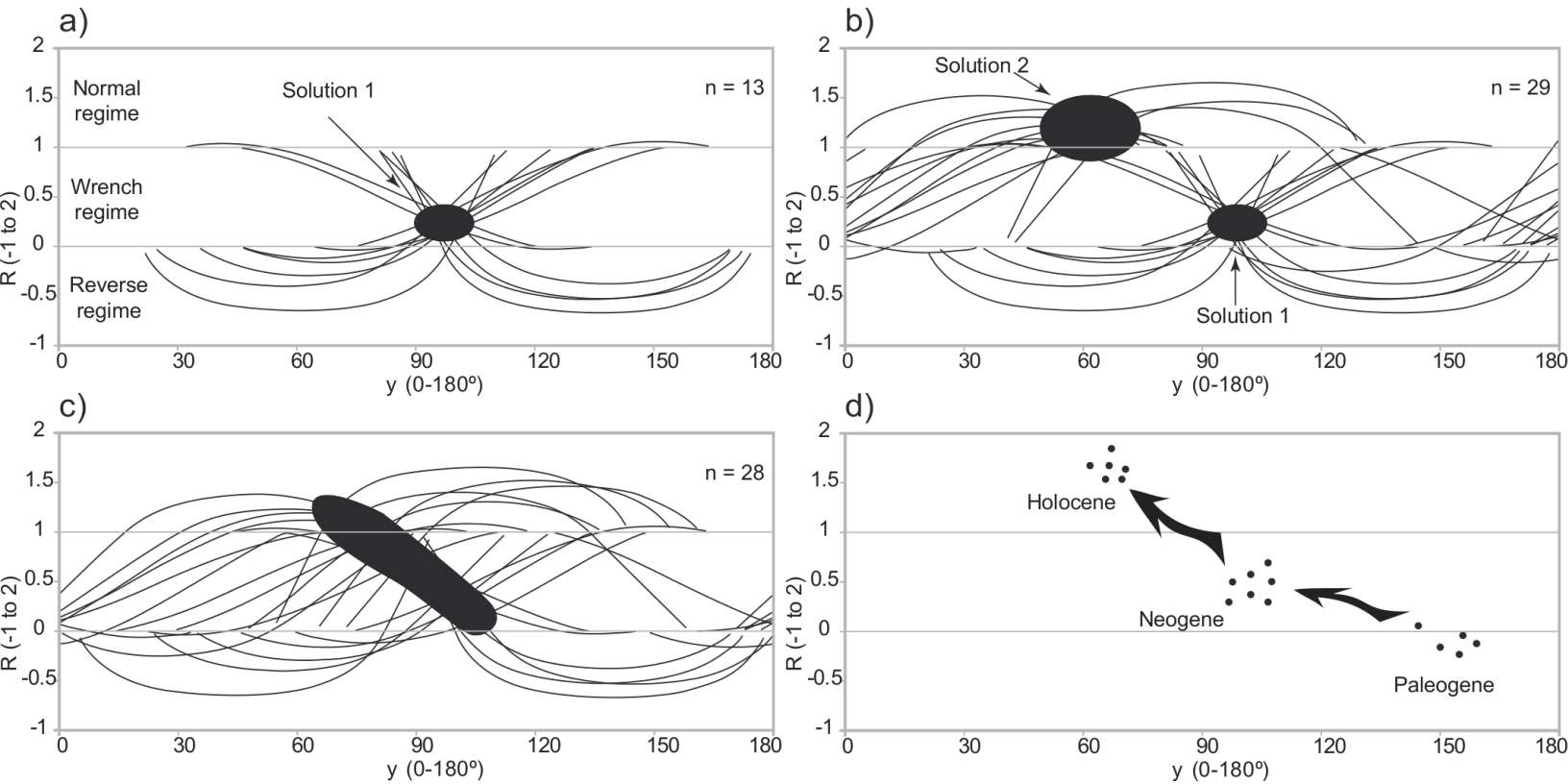
a)
Normal regime
Wrench regime
Reverse regime
Solution 1
n = 13
b)
Solution 2
Solution 1
n = 29
c)
n = 28
d)
Holocene
Neogene
Paleogene
R (-1 to 2)
y (0-180º)

Figure4

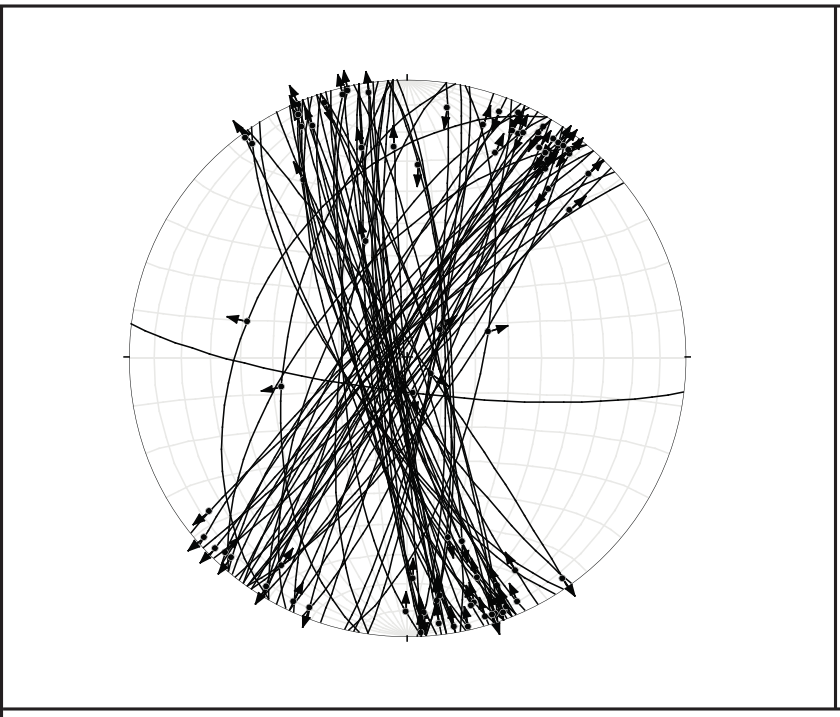

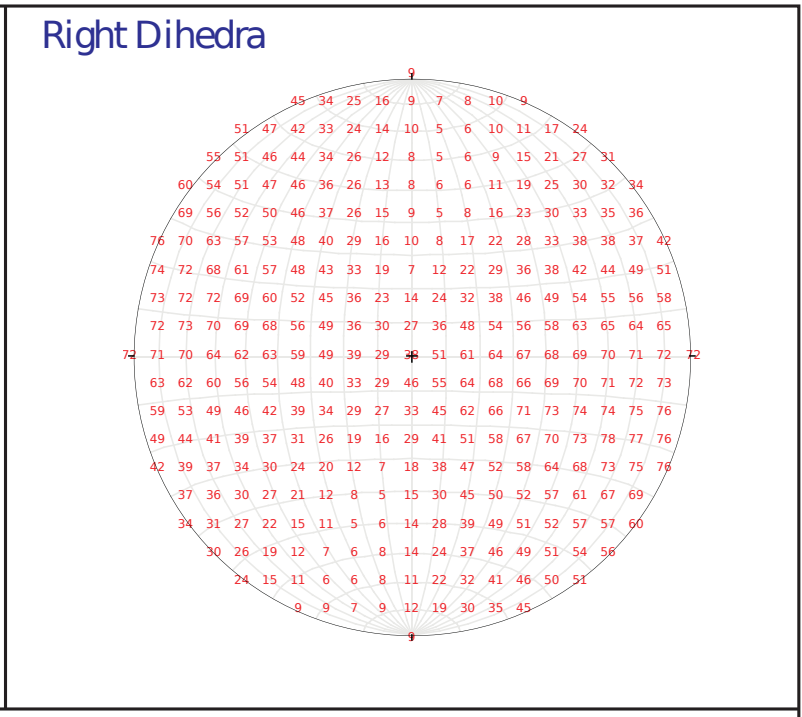
Right Dihedra

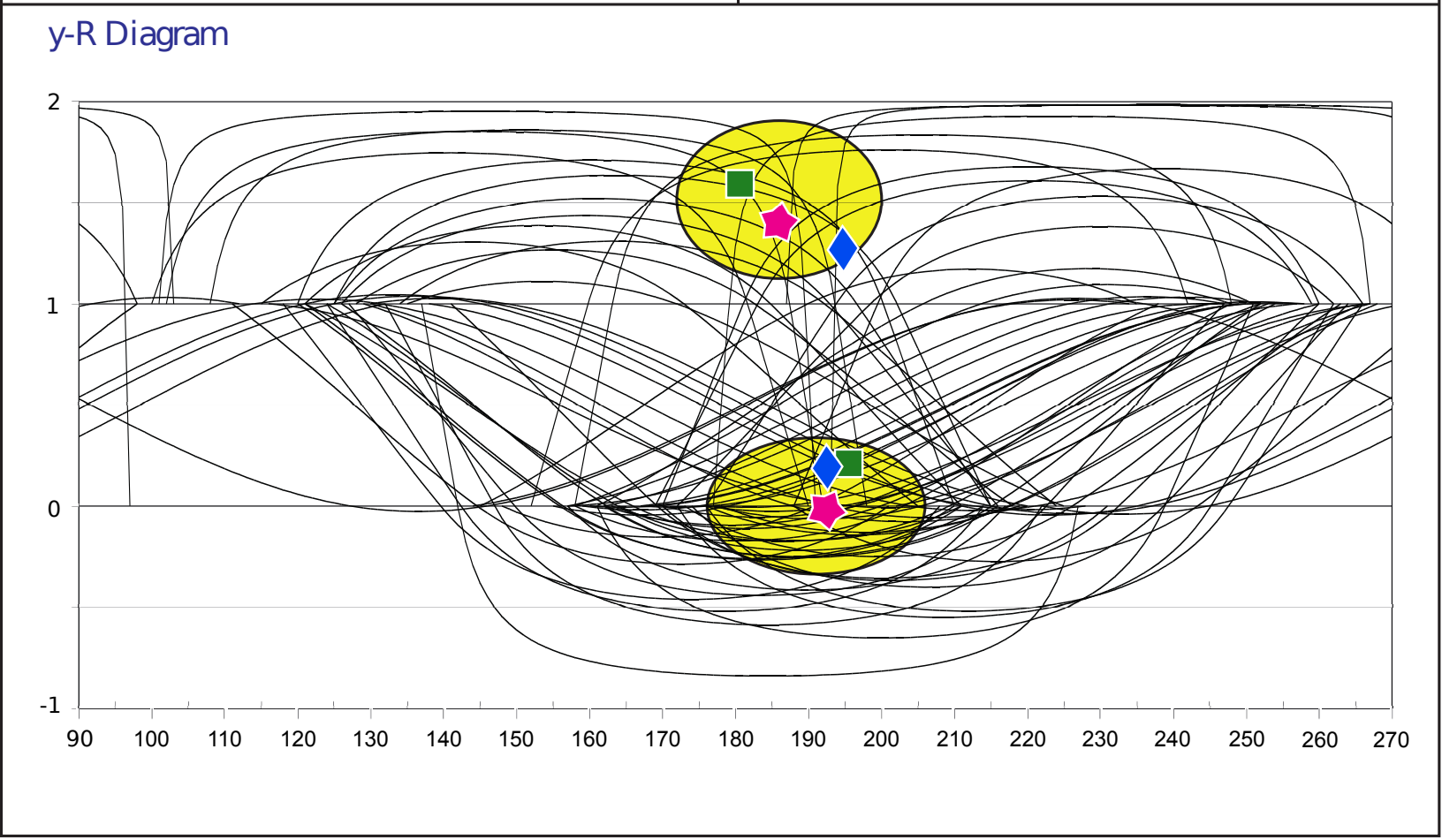
y-R Diagram
2
1
0
-1
90
100
110
120
130
140
150
160
170
180
190
200
210
220
230
240
250
260
270

Computer Code

Click here to download Computer Code: Computer Code.doc